

## Intermediate range order and structure in colloidal dispersions with competing interactions

P. Douglas Godfrin, Ramón Castañeda-Priego, Yun Liu, and Norman J. Wagner

Citation: *The Journal of Chemical Physics* **139**, 154904 (2013); doi: 10.1063/1.4824487

View online: <http://dx.doi.org/10.1063/1.4824487>

View Table of Contents: <http://scitation.aip.org/content/aip/journal/jcp/139/15?ver=pdfcov>

Published by the [AIP Publishing](#)

---

### Advertisement:



## Re-register for Table of Content Alerts

Create a profile.



Sign up today!



# Intermediate range order and structure in colloidal dispersions with competing interactions

P. Douglas Godfrin,<sup>1</sup> Ramón Castañeda-Priego,<sup>2</sup> Yun Liu,<sup>1,3</sup> and Norman J. Wagner<sup>1,a)</sup>

<sup>1</sup>Center for Neutron Science, Department of Chemical and Biomolecular Engineering, University of Delaware, 150 Academy St, Newark, Delaware 19716, USA

<sup>2</sup>División de Ciencias e Ingenierías, Universidad de Guanajuato, Loma del Bosque 103, 37150 Leon, Mexico

<sup>3</sup>NIST Center for Neutron Science, National Institute of Standards and Technology, Gaithersburg, Maryland 20899, USA

(Received 6 July 2013; accepted 25 September 2013; published online 18 October 2013)

Colloidal dispersions with a short-range attraction and long-range repulsion can exhibit an intriguing intermediate range order, manifested in scattering experiments as a low- $q$  peak in the structure factor. Monte Carlo simulations are performed on fluids that exhibit intermediate range order to explicitly determine its connection to a possible state of microphase separation, equilibrium clustering. This is accomplished by decomposing the structure factor into cluster-cluster, monomer-monomer, and cross-correlations that cannot be extracted from experimental scattering patterns. Our simulation results indicate that the intermediate range order arises from either monomeric or cluster species, depending on solution conditions, and reflects the presence of a preferred length scale that is not trivially related to the interparticle potential. Further, criteria are established to define monomer, cluster, and percolated states in these systems that facilitate further studies. Combining scattering techniques with simulations provides an effective method for identifying clustered states in complex fluids. © 2013 AIP Publishing LLC. [<http://dx.doi.org/10.1063/1.4824487>]

## I. INTRODUCTION

Colloidal dispersions with a short-range attractive and long-range repulsive (SALR) potential are of great scientific interest as they are related to many important applications such as spontaneous patterning<sup>1,2</sup> and protein cluster formation of membrane proteins,<sup>3,4</sup> globular proteins,<sup>5-7</sup> and therapeutic monoclonal antibodies.<sup>8,9</sup> The competition of these two potential features provides a diverse set of structural states that offer opportunities to engineer desirable properties of colloidal systems. Therefore, formulating new materials from such systems will benefit from developing a direct connection between dispersion microstructure (and its associated properties) and the inter-particle potential.

Among the numerous solution microstructures created by the two competing potential features, the formation of equilibrium, dynamic clusters in solution have been investigated intensively. Dynamic clusters are reversible aggregates with a finite size and polydispersity, which coexist at equilibrium in solution with individually dispersed particles.<sup>10-13</sup> Such equilibrium clusters are to be distinguished from fractal aggregates and coagulates that form irreversibly when a dispersion is destabilized, growing until all particles are consumed and the system percolates or sediments.<sup>14,15</sup> In a clustered state, the short-range interparticle attraction drives particles to form clusters whose size is limited by the long-range repulsive potential. The strength of the short-range attraction is not so significant, such that clusters re-disperse as monomers

upon dilution. Both simulations and theoretical calculations demonstrate that, for the right combination of potential parameters, clusters will grow until they stabilize to form Wigner crystals or glasses comprised of clusters.<sup>10,11,16</sup> For less repulsive inter-cluster interactions, clusters can gel with increasing volume fraction.<sup>7,10,12,16-19</sup> Thus, clustered states can exhibit many properties similar to those found for traditional colloidal dispersions.

Experimental observations of clustered states formed by  $\mu\text{m}$  sized colloidal particles have been reported.<sup>5,7,17,18</sup> However, the experimental investigation of cluster formation by small particles, such as proteins, is much more challenging and remains an active area of research, especially given the potential importance of such states for biological therapeutics.<sup>20</sup> Clustering in aqueous lysozyme protein solutions was inferred from small angle neutron scattering (SANS) measurements.<sup>5-7,21-23</sup> Under specific conditions, scattering patterns of these systems exhibit a peak in the inter-particle structure factor at small scattering angles, or  $q$ -values,<sup>5-7,23</sup> where  $q$  is the momentum transfer or scattering vector. The simultaneous study of colloidal and lysozyme systems initially linked this low- $q$  peak to the formation of clusters with a well-defined size, where the low- $q$  peak was attributed to the correlation of stable clusters in solution.<sup>5</sup> Investigations using liquid state theory have augmented this proposed relationship over a range of inter-particle potential parameters.<sup>24-27</sup> However, the presence of a scattering peak only signifies the presence of a correlation length between scattering centers in a sample and, as such, does not directly indicate the presence of clusters as commonly defined. Consequently, this low- $q$  peak has recently been suggested to arise

<sup>a)</sup> Author to whom correspondence should be addressed. Electronic mail: [wagnernj@udel.edu](mailto:wagnernj@udel.edu).

from the formation of *intermediate range order* (IRO) between scattering centers, of which a structured fluid consisting of clusters of particles is only one specific scenario.<sup>23</sup> Rather than referring to this anomalous scattering peak as the “cluster peak,” it has been termed an “intermediate range order peak” to more properly reflect the general structural order it represents.

While scattering patterns sum contributions from all scattering centers, it is desirable to distinguish the contributions from specific particles, such as those contained in clusters. Liquid state integral equation theory (IET) and small angle scattering experiments provide ensemble averages without the means to make such distinctions. Direct particle simulations, however, provide particle-level details of the cluster size distributions and corresponding contributions to the scattering pattern. By distinguishing cluster and monomer species, the contributions leading to the IRO peak can be explicitly calculated.

The goal of this study is to understand the relationship between monomer and cluster correlations within the solution and the formation of an IRO peak in the scattering structure factor. To achieve this, we use Monte Carlo (MC) simulations to study a model system with realistic parameter values across a range of state points to assess the validity of using the IRO peak as an indicator of cluster formation. The microstructures for a series of states exhibiting IRO are decomposed into contributions arising from monomer, cluster, and cross correlations. We propose a new method of identifying the state conditions at which clustered fluids exist based on the cluster distribution. This method enables us to define unambiguously monomer states, cluster states, random percolated states, and cluster percolated states. This leads to a classification, or taxonomy, of states and a method by which to identify these states in practice. The structure of each state and its relation with the IRO peak are discussed in detail.

## II. NUMERICAL CALCULATIONS AND SIMULATION DETAILS

MC simulations<sup>28,29</sup> were performed with 1728 particles in a cubic box with periodic boundary conditions in the NVT ensemble. A homogeneously distributed cubic lattice was generated as the initial configuration. The simulations were conducted in steps, with a step consisting of an attempt to move a single randomly selected particle. Each system was thermalized for  $2 \times 10^7$  steps, during which the configurational energy was tracked to ensure equilibration. Thermodynamic and structural quantities were averaged over a run of  $2 \times 10^7$  steps, of which  $4 \times 10^4$  independent configurations were used to calculate cluster properties and percolation statistics. The initial single move displacement distance of 0.1, where all distances are normalized by the particle diameter  $\sigma$ , was dynamically adjusted to maintain an acceptance ratio of 30%.

Particles interact via a central force pair wise potential, as shown in Fig. 1, as a particular type of a hard sphere double Yukawa (HSDY) interaction potential:

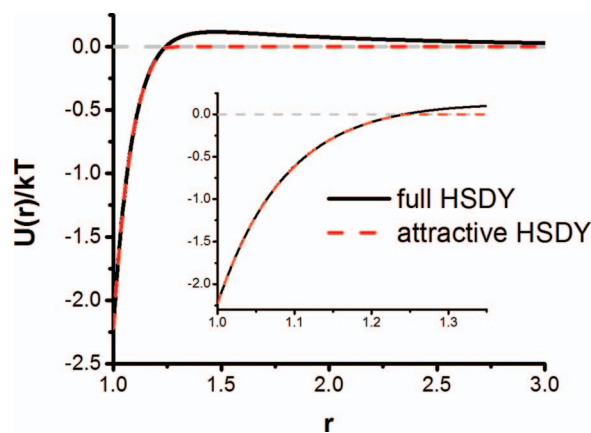


FIG. 1. The interaction potential used in the MC simulations is given by the black line. The reference attractive potential (red dotted line) is used to estimate the onset of phase separation, represented by the binodal.

$$\frac{U(r)}{kT} = \begin{cases} \infty & r < 1 \\ \left( \frac{1}{T^*(1-\lambda)r} \right) (-e^{-z_1(r-1)} + \lambda e^{-z_2(r-1)}) & r \geq 1 \end{cases} \quad (1)$$

where  $r$  is the reduced particle-particle separation,  $z_1$  is the inverse range of attraction,  $z_2$  is the inverse range of repulsion,  $\lambda$  is the ratio of strength of repulsion to attraction, and  $T^*$  is the reduced temperature.  $T^*$  represents the relative magnitude of the potential energy well depth to thermal energy, as defined previously for the SALR-HSDY potential,<sup>30</sup> calculated explicitly as  $(K_1 - K_2)/k_B T$ , where  $K_1$  and  $K_2$  are the strengths of attraction and repulsion, respectively. The double Yukawa potential is a widely studied model potential chosen for its successful representation of protein and micellar solutions and thus, its applicability to experimentally relevant systems.<sup>22,31</sup> Though the model potential is not derived from specific molecular interactions, it is widely adopted for studies because with an appropriate selection of parameters, it quantitatively represents the total effective force acting between particles.<sup>32</sup> Further, Noro and Frenkel showed that in the limit of short-range attraction, as employed here, the second virial coefficient is the important, defining characteristic rather than the specific form of attraction.<sup>33</sup>

The set of potential parameters of  $\lambda = 0.1$ ,  $z_1 = 10$ , and  $z_2 = 0.5$  are used for the simulations in this work.  $z_1$  is chosen based on the relative interaction range of a short-range attraction observed among globular proteins.<sup>23,30</sup> Under these conditions an IRO peak has been observed in the structure factor over a range of reduced temperatures and volume fractions by previous studies.<sup>26,30,34</sup> Here, the radial distribution function  $g(r)$  and structure factor  $S(q)$  of the system are calculated by direct summation and averaged over the trajectory using standard methods.<sup>28,29</sup> Below a reduced temperature of 0.25, the system energy and pressure could not reach a thermodynamically stable state after  $1 \times 10^8$  simulation steps, so that 0.25 is the practical lower limit for these investigations. The reason for this is elucidated within the context of the reference state in Sec. III.

The attraction component of the potential is taken as a reference potential, shown in Fig. 1, and defined as

$$\frac{U^{ref}(r)}{kT} = \begin{cases} \infty & r < 1 \\ \left( \frac{1}{T^*(1-\lambda)r} \right) (-e^{-z_1(r-1)} + \lambda e^{-z_2(r-1)}) & 1 \leq r \leq r_c \\ 0 & r > r_c \end{cases} \quad (2)$$

The cut-off distance,  $r_c$ , is defined here as the separation at which the HSDY potential first reaches net zero interaction energy beyond the attractive well:  $r_c = 1.2424$ . It is independent of temperature and is intuitively related to the range of attraction that drives particle aggregation. Connectivity is defined by this cut-off distance as particles experiencing an attractive potential with their neighbor. Note that groupings or clusters of particles arise naturally in any fluid state regardless of interactions simply due to density fluctuations,<sup>35,36</sup> and so, an arbitrary definition of cut-off distance can produce clustering and percolation without physical significance. A careful study of this choice of  $r_c$  presented in the supplementary material<sup>60</sup> shows the validity of this choice and consequences of using other values.

Particles less than a distance  $r_c$  from a neighbor are defined as belonging to a specific cluster. Particles not belonging to a cluster of 2 or more particles are referred to as *monomers*. This calculation determines the fraction of particles in clusters and as monomers as well as the amount of clusters of each size (cluster size distribution). The cluster size distribution,  $n(s)$ , is normalized by the cluster size,  $s$ , and system size,  $N_p$ ,

$$N(s) = (s/N_p)n(s) \quad (3)$$

similar to that proposed by Stauffer<sup>37</sup> and used by Chen *et al.*<sup>38</sup> This function represents the average fraction of particles contained in clusters of size  $s$  as opposed to the average number of clusters of  $s$  particles existing in the system. The former provides a normalized function for all cluster sizes, while the latter is biased towards smaller cluster sizes. The normalized cluster size distribution,  $N(s)$ , henceforth referred to as the *cluster size distribution*, is used to identify the state of the fluid at each state point.

Identification of clusters and monomers enables defining a pseudo-two-component fluid comprised of monomers and clusters. This enables calculating the total structure factor with respect to the partial structure factors for each pseudo-component as<sup>39</sup>

$$S(q) = x_M S_{MM}(q) + x_C S_{CC}(q) + 2(x_M x_C)^{\frac{1}{2}} S_{MC}(q). \quad (4)$$

Here, subscripts represent the type of particle (M for monomers and C for particles in a cluster),  $x_i$  represents the fraction of each type of particle in the current configuration of the system, and the structure contributions arise from the monomer-monomer,  $S_{MM}(q)$ , monomer-cluster,  $S_{MC}(q)$ , and cluster-cluster,  $S_{CC}(q)$ , correlations. By definition, correlations involving clusters are calculated by summing over each individual particle within a cluster. Therefore,  $S_{CC}(q)$  is to be distinguished from a correlation between the centers of mass of the clusters in solution.

The three partial structure factors are calculated by the relationship between the structure factor and the radial

distribution function

$$S_{ij}(q) = \delta_{ij} + \rho (x_i x_j)^{\frac{1}{2}} \int_0^\infty \frac{\sin(qr)}{qr} [g_{ij}(r) - 1] 4\pi r^2 dr, \quad (5)$$

where  $\delta_{ij}$  is the Kronecker delta and  $\rho$  is the fluid density. The radial distribution function of each contribution is calculated according to

$$g_{ij}(r) = V^2 \left\langle \sum_{i=1}^{n_i} \sum_{j=1}^{n_j} \frac{\delta(r_{ij} - r)}{n_i n_j V} \right\rangle, \quad (6)$$

where subscripts (i,j) represent the component,  $n$  is the number of particles of each component in a given configuration, and  $V$  is the volume. The radial distribution function for the fluid composed of all particles is defined as

$$g(r) = \frac{V^2}{N^2} \left\langle \sum_{i=1}^N \sum_{j=1}^N \frac{\delta(r_{ij} - r)}{V} \right\rangle. \quad (7)$$

Cluster-cluster correlations,  $S_{CC}(q)$ , can be further decomposed into intra- and inter-cluster correlations by counting only those particles within the same or different clusters, respectively.

Each sampled configuration is tested for percolation, defined as when a cluster spans the entire system size in at least one dimension. Such a cluster is effectively infinite in size when periodic boundary conditions are employed and is denoted as a *percolated cluster*. Percolation at a given state point is defined when at least 50% of the configurations sampled contain at least one percolated cluster.<sup>40</sup> States that fulfill this criterion can be further distinguished as “cluster percolated” states, rather than monomer percolated states, which will be discussed later in the paper. Although percolation depends on the size of the simulation box, information in the supplementary material<sup>60</sup> shows these are not significant for our results.

The liquid-liquid phase separation (binodal) of the reference attractive potential is generated using discrete perturbation theory (DPT) calculations.<sup>41–45</sup> DPT represents the interaction potential by numerous discrete square well-like steps and is known to calculate accurate gas-liquid binodals and critical points. As an estimate of the percolation transition, the reference potential is mapped to a square well potential according to the Noro-Frenkel extended law of corresponding states.<sup>33</sup> With the known critical temperature and volume fraction, the critical reduced second virial coefficient,  $B_{2c}^*$ , can be calculated and used to determine the effective range of a square well potential,  $\delta$ , according to

$$1 + \delta = \left( 1 - \frac{1 - B_{2c}^*}{1 - \exp\left(\frac{1}{T_c^*}\right)} \right)^{1/3}. \quad (8)$$

The percolation transition line is finally calculated by first determining the Baxter parameter,<sup>46,47</sup>  $\tau$ , which is representative of the strength of attractive interactions, and implementing it in Eq. (24) of Miller and Frenkel<sup>46</sup> as follows:

$$\rho_{\text{perc}}(\tau) = \frac{-10.09 + 182.4\tau + 606.9\tau^2 + 15.31\tau^3}{1.0 + 507.9\tau + 548.9\tau^2}. \quad (9)$$

### III. RESULTS AND DISCUSSION

Simulations are performed on six state points exhibiting an IRO peak in  $S(q)$ , which are located on the phase diagram of the reference system in Fig. 2. States are determined according to the cluster size distribution and fraction of percolated configurations and are classified as monomer dominated (A, B), clustered (C), cluster percolated (D), and random percolated (E, F), whose definitions will be discussed later in the paper. While the binodal of the SALR-HSDY potential is difficult to calculate, it is known that the addition of a long-range repulsion to attractive potentials shifts the liquid-liquid coexistence region to lower temperatures.<sup>48</sup> Correspondingly, all studied states are in the one phase fluid region for the SALR-HSDY potential.

Monomer dominated states transition to clustered states upon lowering temperature. Increasing concentration causes these states to transition to percolated states and cluster percolated states, respectively. The percolation transition of the reference attractive system sits within the region of the state diagram where the SALR-HSDY system transitions from a monomer dominated to percolated state. Interestingly, a clustered and a cluster percolated state are found within the binodal of the reference state diagram. The results shown here suggest that the binodal of an appropriately defined reference attractive potential may act as an indicator of the onset of cluster formation. This hypothesis will be explored further in a future investigation.

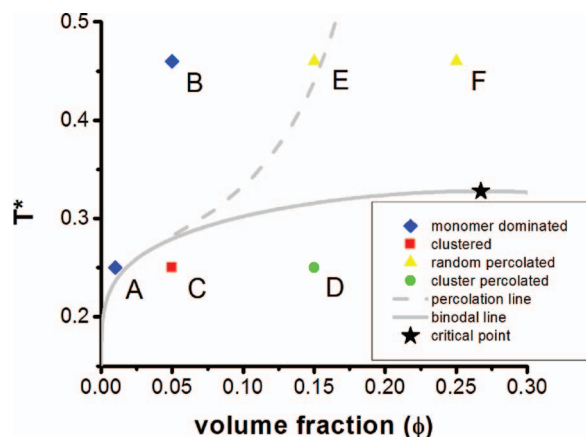


FIG. 2. The phase diagram shows the relative location of six state points of a HSDY fluid with  $z_1 = 10$ ,  $z_2 = 0.5$ , and  $\lambda = 0.1$ . The state points represent monomer dominated systems (blue diamonds), clustered systems (red squares), cluster percolated systems (green circles), and percolated networks (yellow triangles). The reference attractive potential, outlined in the text, is used to estimate the binodal (grey solid line) and percolation transition (grey dotted line).

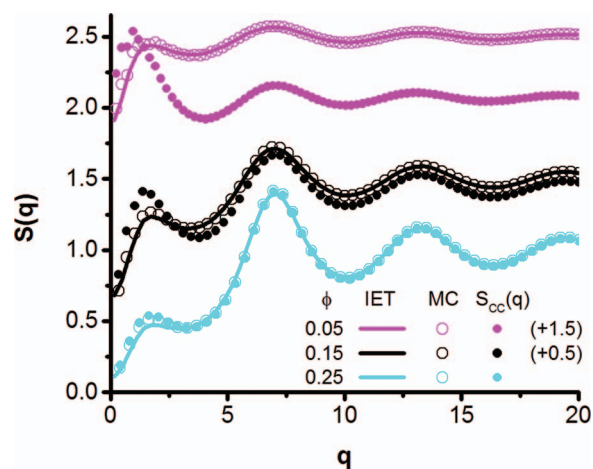


FIG. 3. The relative contributions of cluster-cluster correlations  $S_{cc}(q)$  (filled dots) to  $S(q)$  (open dots) are shown for systems at a reduced temperature of  $T^* = 0.46$  and three volume fractions (0.05, 0.15, 0.25) corresponding to states B, E, and F. An IRO peak appears for all states.  $S(q)$  results are compared with IET calculations using a thermodynamically consistent closure relation (solid lines).

Three of these state points (at a constant  $T^*$  of 0.46) are shown in Fig. 3 to highlight the trend in the magnitude of their IRO peaks. The total structure factor and the partial structure factor of particles in clusters (i.e., cluster-cluster correlations) obtained from MC simulations are given for states B, E, and F. The dependence of IRO peak formation on temperature and volume fraction has been studied previously by integral equation theory.<sup>24,26,30,34</sup> These studies have assumed that a direct connection exists between the formation of an IRO peak and the formation of a clustered state. In contradiction to this assumption, all three states studied here exhibit an IRO peak, where the magnitude clearly decreases with increasing volume fraction and simultaneously, cluster-cluster correlations,  $S_{cc}(q)$ , are an increasingly large contribution to the total structure. These results show that the IRO peak does not trivially indicate a correlation between particle clusters and hence, in agreement with previous researchers,<sup>7</sup> it is incorrect to refer to it as a “cluster peak.” Rather, this low- $q$  feature in the scattering arises from a complex combination of correlations of monomers and particles in clusters as well as their cross-correlations. In the following, we exploit the particle-level detail of MC simulations to study the relationship between microstructure and features of the IRO peak in the structure factor.

#### A. State definitions and microstructures

The cluster size distributions and average fraction of clustered and percolated particles of all six states are shown in Figs. 4(a) and 4(b), respectively. The cluster size distribution distinguishes monomer and clustered states. The aforementioned method of determining percolated clusters is used to identify a percolated state. By combining the cluster size distribution, percolation criterion, and details of the inter-particle structure, a *cluster percolated state* can also be defined. In this state, the percolated cluster is comprised of well-defined particle clusters, in contrast to the usual random percolation state.

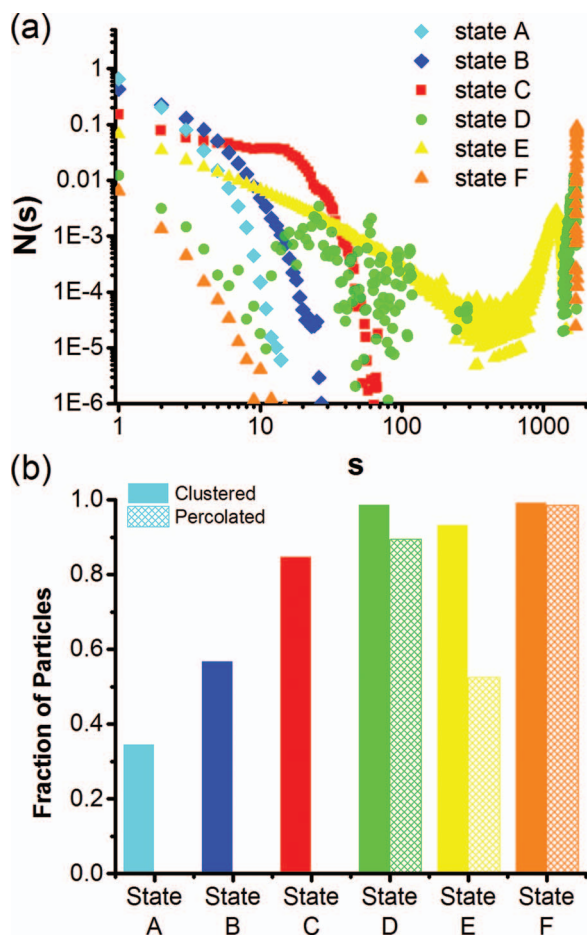


FIG. 4. (a) Cluster size distributions are given for all six states studied: monomer-dominated – state A ( $\phi = 0.01$ ,  $T^* = 0.25$ ) and state B ( $\phi = 0.05$ ,  $T^* = 0.46$ ); clustered – state C ( $\phi = 0.05$ ,  $T^* = 0.25$ ); cluster percolated – state D ( $\phi = 0.15$ ,  $T^* = 0.25$ ); percolated – state E ( $\phi = 0.15$ ,  $T^* = 0.46$ ) and state F ( $\phi = 0.25$ ,  $T^* = 0.46$ ). (b) The average fraction of particles contained in a cluster (clustered) and contained in a percolated cluster (percolated) are given for each of the same six states with the same colors from (a).

An  $N(s)$  monotonically decreasing with cluster size defines a “monomer state.” The most probable species are monomers and there is no preferred cluster size within the distribution. Note that this is similar to a hard-sphere fluid, as shown further in the supplementary material.<sup>60</sup> Both state points A and B have a monotonically decreasing distribution of cluster sizes and the probability of finding clusters increases with concentration, as expected. These are defined as monomer dominated fluids. However, when the cluster size distribution develops a probability maximum at a size larger than a monomer, the state is defined as a cluster fluid, such as state point C. Previous studies have defined clustered states by the average cluster size,<sup>7,49</sup> however, monomers may be the most abundant species in solution by this definition. Requiring clustered fluids to exhibit a peak in  $N(s)$  ensures the properties of these states result from the dominant cluster species. State C, the clustered state, has almost 85% of particles in clusters with most of those being roughly the most preferred size of around 12 particles. The finite peak in the cluster size distribution indicates a dominating size scale, albeit very polydisperse, in the solution structure. Note that a

percolated state exhibits a large peak at a large  $s$  value corresponding to the box size, but this should not be confused with the cluster peak defined as a local maximum in  $N(s)$  indicating the formation of finite-size particle clusters.

When at least 50% of configurations within a simulation trajectory exhibit a percolated cluster the state is identified as percolated. As seen from Fig. 4(a), the cluster size distributions of states D, E, and F all have a peak at large cluster sizes near the system size of 1728 particles due to percolation. According to Fig. 4(b), at least 93% of particles in each of the percolated states are part of a cluster, with varying amounts of those contributing to the percolated cluster.

Although the features presented in Fig. 4(b) cannot distinguish the three percolated states, their cluster size distributions differ in shape. In particular, the cluster size distribution for state D exhibits a local maximum at roughly the same preferred size as state C, which is at a lower volume fraction but the same temperature. This distinguishes state D from states E and F, which have cluster size distributions typical of percolated fluids. Indeed, the microstructure of state D is fundamentally different from that of states E and F, despite all three exhibiting percolation. Progressively increasing the volume fraction from state B to E and F leads to percolation as would be qualitatively expected for a fluid with attractive interactions or even a hard-sphere fluid.<sup>35,50,51</sup> However, upon lowering the temperature to the region under the binodal line of the reference system, the SALR-HSDY system forms clusters with a preferred size. Further concentration of the system leads to percolation of these clusters. Thus, at this lower temperature, the long-range repulsion leads to a preferred length scale associated with frustrated phase separation that sets the microstructure of the percolated state. This difference could be important for the material properties of gels and glasses formed from such systems, such as ceramics (i.e., green body), zeolites,<sup>52–54</sup> and membranes<sup>3,4</sup> that use these as intermediates.

To further illustrate the difference between a random percolated state and a cluster percolated state, the cut-off distance is artificially varied to better show the connectivity. Systematically increasing the cut-off distance probes the length scale dependence of local order and provides insight into the microstructure and particle correlations. Note that the actual microstructure does not vary, just the definition of cluster membership. Figs. 5 and 6 illustrate the trends in the cluster-cluster rdf and characteristic particle configurations with cut-off distance for the cluster percolated and random percolated states D and E. Corresponding cluster size distributions can be found in the supplementary material.<sup>60</sup> A single configuration with a representative cluster size distribution of the average for each percolated state is selected for the analysis. Configuration snapshots show only particles that are part of clusters and each cluster is labelled with a different color.

When comparing the microstructure of states D and E (Figs. 5(f) and 6(f)), the cluster percolated state D appears to have a more ordered network that is similar to states found previously in experiment<sup>16</sup> and simulation.<sup>10</sup> Quantitatively, this order is evident by a pronounced doublet near  $r = 1.8$  and a smaller peak at  $r = 2.6$  in the cluster-cluster rdf (Figs. 5(c)

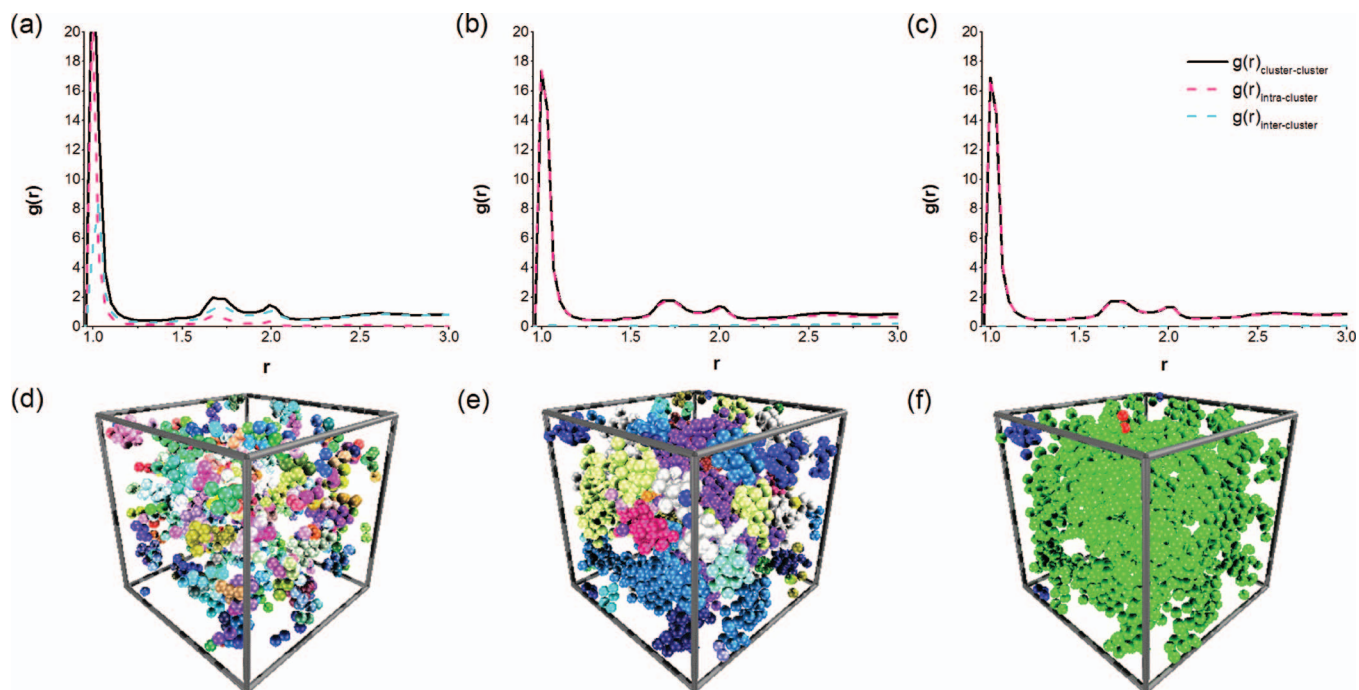


FIG. 5. The cluster-cluster rdf as well as the intra-cluster and inter-cluster rdf are shown for cut-off distances of (a) 1.005, (b) 1.035, and (c) 1.2424 for state D. The snapshots (d)–(f) are of a characteristic configuration with the corresponding  $r_c$  of the plot above and show particles within a given cluster as the same color.

and 6(c)). These peaks help to distinguish state D from the other two percolated state as a cluster percolated state.

The intermediate range peaks in the cluster-cluster rdf of state D are present for all choices of cut-off distance (Fig. 5). At a small cut-off distance of 1.005, the structure is already dominated by clusters. Further increase of the cut-off distance to 1.035 and 1.2424 shifts the preferred cluster size

to larger sizes until a system spanning percolated cluster is evident. Interestingly, the location and magnitude of the peaks in  $g(r)$  change little over this variation in cut-off distance indicating that the particle-level microstructure of state D is relatively homogeneous through the clustered fluid. This analysis supports a mechanism of percolation in state D that results from the merging of clusters upon increasing the

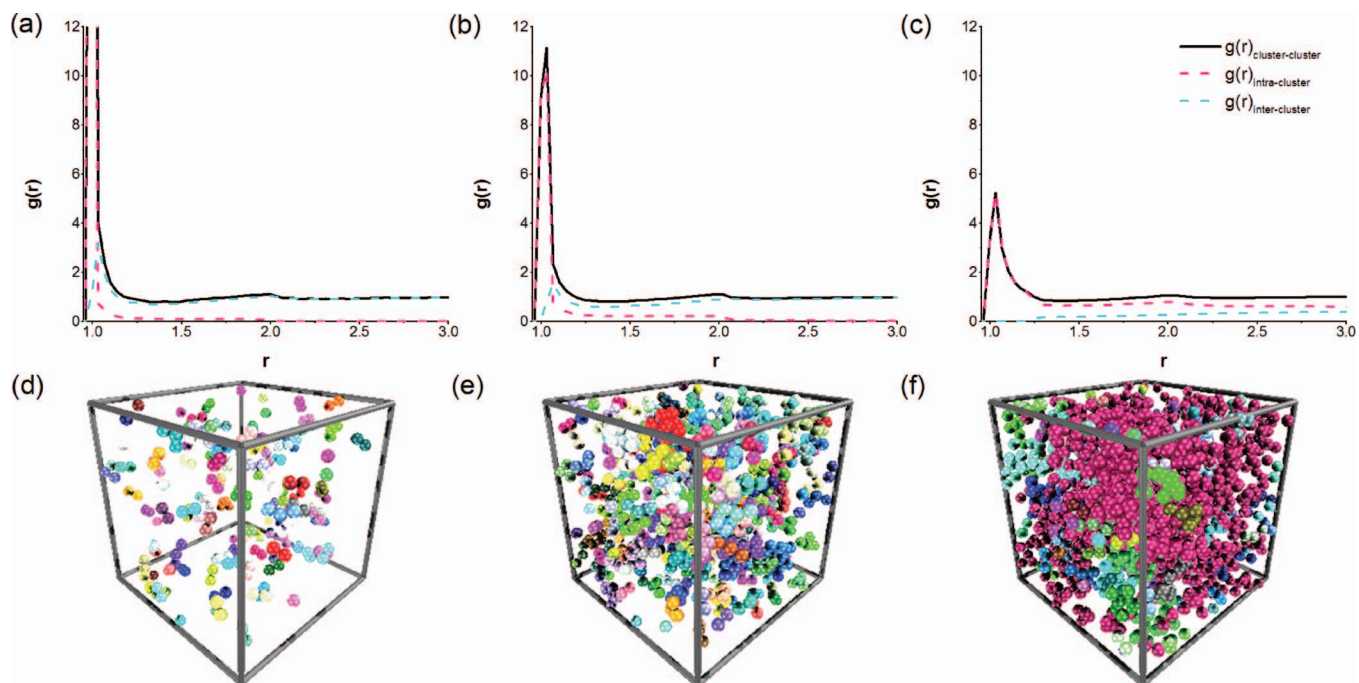


FIG. 6. The same details as given in Fig. 5 are presented for percolated state E. A movie of the evolution of clusters with  $r_c$  is given in the supplementary material<sup>60</sup> for the four non-monomer dominated states.

concentration from the clustered fluid state. This is consistent with the stabilization of clusters at  $T^* = 0.25$  by well-understood cluster-cluster repulsion.<sup>11</sup>

In contrast, the structure of state E in Fig. 6 exhibits a cluster-cluster rdf that contains a peak at contact and a weak, broad peak at  $r = 2.0$  for all bond distances. At the smallest cut-off distance of 1.005, the system is composed mainly of monomers and very small clusters. Upon increasing the cut-off distance to 1.035, more clusters appear with larger size and more polydispersity. Further increase of the cut-off distance to 1.2424 leads to percolation. For each choice of cut-off distance the cluster-cluster rdf is composed mainly of inter-cluster correlations with a small peak just above the bond distance value. Thus, clusters are randomly dispersed in the simulation box. Further, the dramatic drop in magnitude of the contact peak in the cluster-cluster rdf when increasing the cut-off distance is indicative of particle by particle growth of clusters. In contrast, in a percolated cluster state, aggregation of two clusters reduces the number of particles at cluster surfaces, which enhances the number of nearest neighbors and maintains a large contact peak. From this analysis we can conclude that the percolated structure of state E forms from the aggregation of monomers and small polydisperse clusters that eventually span the system. While the IRO peak indicates an inherent internal length scale, the correlations are weaker than those observed for the cluster-percolated state due to the broad size polydispersity of the units that comprise the percolated cluster.

## B. Structure factor decomposition

A summary of the magnitude of the IRO peak in each of the six states is provided in Fig. 7 as a function of temperature and volume fraction. A possible trend appeared between the position of the IRO peak and temperature, summarized in the supplementary material,<sup>60</sup> where states at low temperature consistently formed IRO peaks at smaller  $q$ -values than at higher temperature. Consequently, states along the two isotherms studied here exhibit distinctly different trends in the magnitude of the IRO peak with volume fraction. Below the critical reduced temperature ( $T^* = 0.25$ ), the magnitude of the IRO peak increases with volume fraction, while above  $T_c^*$  ( $T^* = 0.46$ ) the magnitude decreases with increasing volume fraction. Thus, at the lower temperature as clusters form and become more abundant with increasing volume fraction, they become increasingly more ordered or localized. The enhanced order in the IRO peak at increasingly smaller  $q$ -values (larger length scales) for the lower temperature can be attributed to the increasing strength of the repulsive barrier relative to the thermal motion. In contrast, at higher temperatures, where a dominant cluster size does not form, increasing volume fraction produces an increasingly more disordered solution structure on the IRO length-scale. These findings further support the distinction of cluster percolated and randomly percolated states.

The large difference in the magnitude of the IRO peak between the clustered and monomer dominated states (both percolated and fluid) is highlighted in Fig. 7. Both the clustered

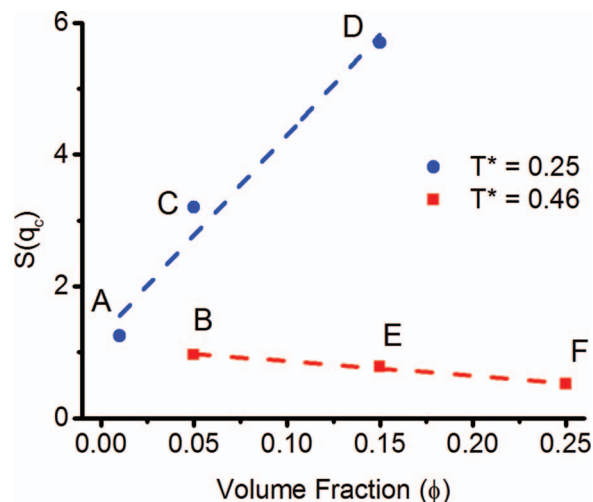


FIG. 7. Magnitudes of IRO peak in the structure factor are shown for state points along the two isotherms studied. The trend in peak height with volume fraction below the critical reduced temperature ( $T^* = 0.25$ ) is distinctly different from the systems outside the two phase region of the reference attractive system ( $T^* = 0.46$ ).

state and the cluster percolated state have a distinctly larger peak than the other states, both of which have an IRO peak magnitude greater than 3. Previously, a large sharp IRO peak ( $S(q) \geq 3$ ) has also only been observed in conjunction with the formation of a peak in the cluster size distribution (i.e., the formation of a cluster phase as defined in this work),<sup>11,12</sup> although this trend was not emphasized. Based on our limited observations and the literature, we hypothesize that the existence of clustered states can be characterized by an IRO peak greater than 3 in magnitude. Further work validating the universality of this possible criterion is on-going.

Monomer-monomer, cluster-cluster, and cross-correlation contributions as well as the total system structure factor are presented in Fig. 8 for each of the six states studied. Each state has a unique combination of these features, which are compared in detail with respect to the structural features outlined in Sec. III A.

The three components of the structure factor for the two monomer states (states A and B) are shown in Figs. 8(a) and 8(b), respectively. Although monomers compose a majority of the species, both states have a structure with a pronounced IRO peak (at  $q \approx 1$ ) relative to the monomer-monomer peak (at  $q \approx 7.3$ ). The magnitude of the IRO peak of these monomer states is actually larger than that of the randomly percolated states (states E and F) despite lacking local structural order as indicated by the small average number of neighbors per particle, presented in the supplementary material.<sup>60</sup> Therefore, it is largely the localization of monomers on this longer length scale that generates the observed IRO peak.

The decomposition of the structure directly demonstrates the large content of monomers in both monomer states. The magnitude of the monomer correlations,  $S_{MM}(q)$ , are roughly 50% of the magnitude of the total structure factor over the full  $q$ -range. Although the correlation of particles in clusters,  $S_{CC}(q)$ , does not compose a clear majority of the magnitude of the total structure, the form of  $S(q)$  (i.e., the presence of an IRO peak) more closely resembles that of  $S_{CC}(q)$ . However,

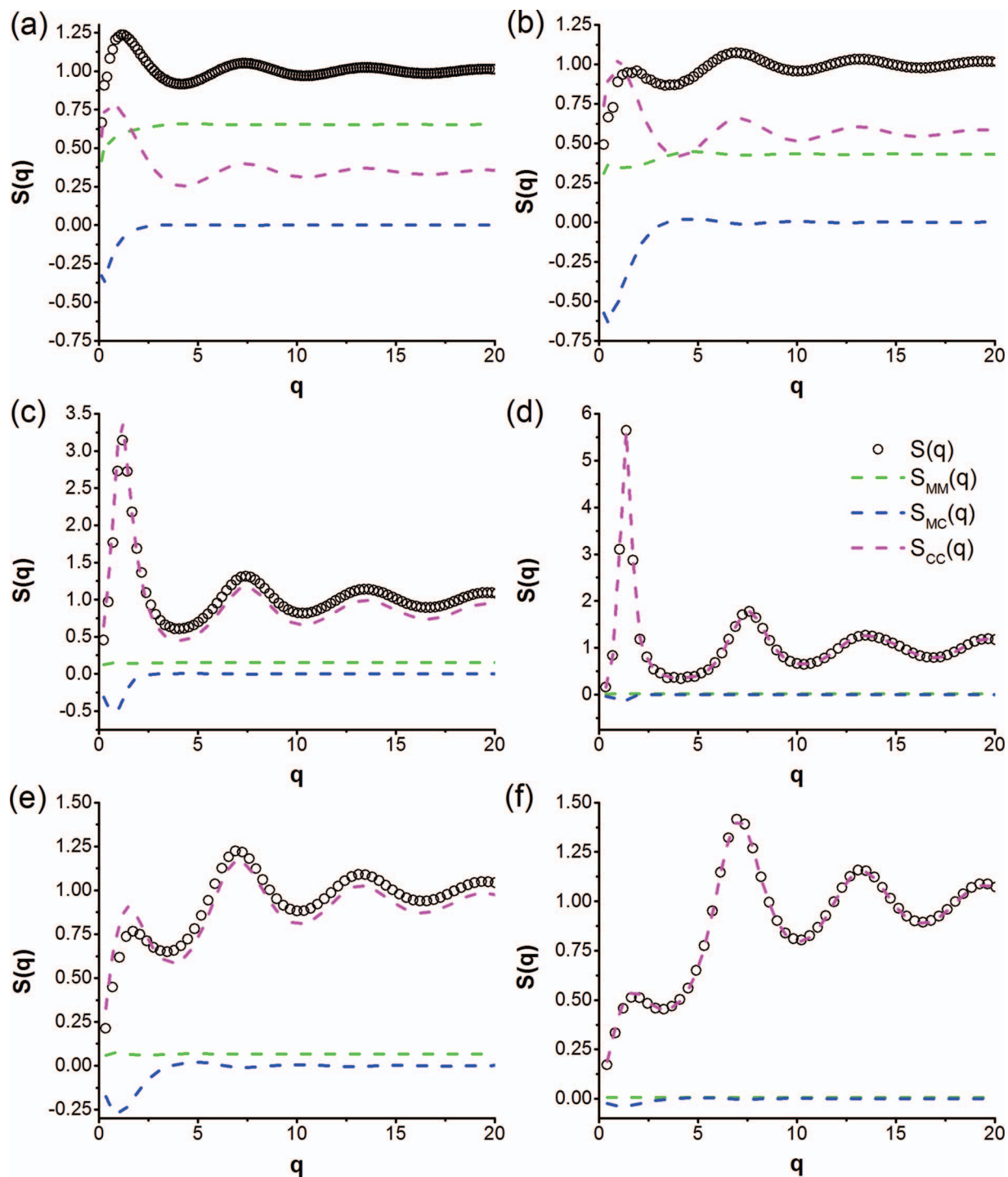


FIG. 8. Structure factors and the three partial structure factor contributions are shown for (a) state A, (b) state B, (c) state C, (d) state D, (e) state E, and (f) state F. The diversity of microstructures that produce an IRO peak is direct evidence of the inaccuracy in using it as an indication of cluster formation.

the location of the IRO peak in  $S_{CC}(q)$  for both state A and B are distinctly shifted from that of  $S(q)$ . This shift is caused by the drop in magnitude of  $S_{MM}(q)$  and correlations between monomers and particles in clusters,  $S_{MC}(q)$ , at small  $q$ -values. Thus, the preferred length scale represented by the IRO peak in  $S(q)$  is a complex combination of monomer and cluster correlations in solution. Interestingly, state B, which has roughly 50% more clusters in solution relative to state A, has a more significant peak in  $S_{cc}(q)$  but a smaller total magnitude of the IRO peak in  $S(q)$  relative to state A. Further detailed

discussion of this is provided in the supplementary material.<sup>60</sup>

Fig. 8(c) shows the partial structure factors for state C. Cluster-cluster correlations clearly dominate the total structure factor and are largely responsible for the IRO peak. The IRO peak has a magnitude of roughly 3.3, which is larger than the Hansen-Verlet criterion for crystallization (2.85);<sup>55,56</sup> however, our simulations and previous findings for SALR-HSDY systems with short-range attraction ( $z_1 \geq 8$ )<sup>57</sup> show no evidence of crystallization under

conditions that produce IRO peaks above the Hansen-Verlet criterion. Although Ref. 56 has demonstrated that the Hansen-Verlet criterion is indeed applicable to SALR-HSDY systems, crystallization is avoided with a short enough range of attraction. Presumably the delicate balance of short-range attraction and long-range repulsion needed to form intermediate range order produces sufficient polydispersity (i.e., in the terminology of Ref. 56, a low enough residual multi-particle entropy) to inhibit crystallization. In the case of a clustered state (state C), the polydispersity of the cluster size distribution prevents the formation of a Wigner crystal state of clusters.

Under conditions where the cluster size distribution has a defined, preferred size, the IRO peak position can be an estimation of the characteristic spacing between clusters, as reported in the literature.<sup>11</sup> From the location of the IRO peak ( $q = 1.2$ ), the characteristic cluster spacing is estimated to be  $r = 2\pi/q \sim 5.2\sigma$ . Assuming a monodisperse system of clusters of 12 particles, which is the preferred cluster size according to the maximum in  $N(s)$ , the average spacing ( $d \sim \rho_c^{-1/3}$ ) between clusters is estimated as  $5\sigma$ . Thus, the preferred cluster size can be estimated from the location of the IRO peak for state points corresponding to a clustered fluid; however, the results will be misleading if applied more broadly to experimental results for monomer dominated fluids with IRO. The broad polydispersity of clusters and a non-zero contribution from monomer- and cross-correlations are responsible for the general lack of correspondence between the location of the IRO peak in  $S(q)$  and the physical microstructure of the fluid.

As a further demonstration of the difficulty in deducing the solution microstructure directly from the IRO peak consider the decomposition of  $S(q)$  of the cluster percolated state (state D) and the two percolated states (states E and F) as shown in Figs. 8(d)–8(f), respectively. Clearly, cluster correlations are the main contribution to the structure factor. Although the IRO peaks formed by these states are in roughly the same position as in state C, they do not contain a preferred cluster size associated with its corresponding real space length scale. This further indicates the danger in generalizing the presence of an IRO peak to cluster formation.

Considering the large percentage of particles in percolated clusters in states D, E, and F (Fig. 4(b)), as well as the large contribution to  $S(q)$  from  $S_{CC}(q)$ , it is apparent that the IRO peak is mainly due to the intra-cluster correlations. By analyzing the height of the IRO peak in  $S_{CC}(q)$ , the cluster percolated state may also be distinguished from the other two percolated states. Immediately upon increasing the cut-off distance from a particle diameter, the  $S_{CC}(q)$  peak magnitude increases dramatically before reaching a maximum for all three states, which is not necessarily at the percolation transition. Fig. 9 shows the magnitude of the peak in  $S_{CC}(q)$  relative to its maximum value as a function of the cut-off distance relative to the value at which the system is percolated,  $r_c/r_c^{\text{perc}}$  (i.e., the smallest cut-off distance where at least 50% of configurations have a percolated cluster). States D, E, and F percolated at  $r_c/r_c^{\text{perc}}$  values of 1.0422, 1.2141, and 1.0843, respectively. The cluster percolated state reaches the maximum at the onset of percolation then remains relatively constant. However, the cluster-cluster correlation IRO peak

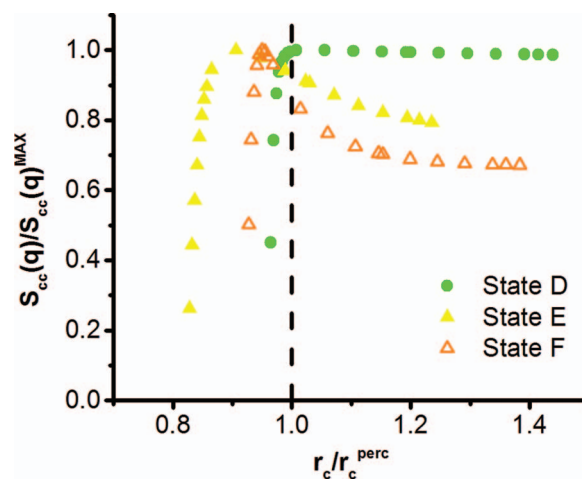


FIG. 9. The height of the IRO peak in the structure factor relative to its maximum value is given as a function of the cut-off distance relative to the cut-off at which 50% of the sampled configurations of that state contain a percolated cluster. The cluster percolated state, D, has a distinctive trend compared to the two monomer percolated states, E and F.

of the two random percolated states reaches a maximum at a cut-off distance before the onset of percolation and slowly decreases until approaching its own plateau. The relatively constant magnitude of the IRO peak with cut-off distance beyond percolation in state D indicates that the characteristic length scale separating clusters is maintained in the network, while randomly percolated states lack any such order.

#### IV. CONCLUSIONS

Monte Carlo simulations of dispersions with IRO identify four distinctly different fluid microstructures that exhibit an IRO peak: monomer dominated, clustered, cluster percolated, and random percolated systems. A new, cluster percolated state can be distinguished from more traditional percolation through examination of the cluster size distribution. These results support IRO as a general occurrence in dispersions with a SALR potential of interaction.

By exploiting the particle-level detail available in Monte Carlo simulations, we have established distinct evidence that the location of the IRO peak is, in general, not an accurate representation of inter-cluster spacing and thus the preferred cluster size. The most accurate method to determine solution structure is to execute MC simulations employing the interaction parameters obtained by fitting experimental scattering patterns using self-consistent IET with an appropriate inter-particle potential. However, our studies suggest a helpful “rule-of-thumb” – clustered and cluster percolated states appear to be associated with IRO peaks with a magnitude of roughly 3 or greater. Under such conditions, the IRO peak may lead to meaningful estimates of average cluster statistics. Further, under conditions conducive to cluster formation ( $T^* < T_c^*$ ), increasing the volume fraction appears to enhance IRO in the system, while the opposite is true for states without distinct cluster formation. These observations may aid in identifying possible clustered states in experiments.

The clustered and cluster percolated states studied here exist within the binodal of a reference attractive system. Cluster formation is shown to be driven by the short-range attraction that produces locally dense regions and corresponds to phase separation for the reference state at these state points. The long-range repulsion suppresses the macroscopic phase separation, resulting in the formation of clusters with a preferred, finite size. The possible connections between the clustered fluid and the phase behavior of the reference attractive system are explored in a forthcoming publication.<sup>58</sup>

Recent experiments have identified three distinct types of clusters depending on their dynamics (transient clusters, dynamic clusters, and permanent clusters),<sup>6,7,23,59</sup> which MC simulations alone cannot distinguish. Future research using kinetic MC and allied techniques will address the interesting questions concerning the lifetime of particles within clusters and the kinetics of cluster formation and disassociation.

## ACKNOWLEDGMENTS

This paper was prepared under cooperative Agreement No. 70NANB10H256 from NIST, U.S. Department of Commerce. The statements, findings, conclusions, and recommendations are those of the author(s) and do not necessarily reflect the view of NIST or the U.S. Department of Commerce. This work has also been supported in part by NSF-Conacyt Grant No. 147892/2011. DPT binodal calculations were provided by Nestor Valadéz-Perez and helpful discussions with F. Sciortino, J. M. Kim, M. Medina-Noyola, A. Stradner, and P. Schurtenberger are acknowledged. We thank a reviewer for helpful comments concerning the presentation of these results.

- <sup>1</sup>M. Seul and D. Andelman, *Science* **267**, 476 (1995).
- <sup>2</sup>R. P. Sear, S. W. Chung, G. Markovich, W. M. Gelbart, and J. R. Heath, *Phys. Rev. E* **59**, R6255 (1999).
- <sup>3</sup>P. Charbonneau and D. Reichman, *Phys. Rev. E* **75**, 050401(R) (2007).
- <sup>4</sup>P. Mulheran, D. Pellenc, R. Bennett, R. Green, and M. Sperrin, *Phys. Rev. Lett.* **100**, 068102 (2008).
- <sup>5</sup>A. Stradner, H. Sedgwick, F. Cardinaux, W. C. K. Poon, S. U. Egelhaaf, and P. Schurtenberger, *Nature (London)* **432**, 492 (2004).
- <sup>6</sup>L. Porcar, P. Falus, W.-R. Chen, A. Faraone, E. Fratini, K. Hong, P. Baglioni, and Y. Liu, *J. Phys. Chem. Lett.* **1**, 126 (2010).
- <sup>7</sup>F. Cardinaux, E. Zaccarelli, A. Stradner, S. Bucciarelli, B. Farago, S. U. Egelhaaf, F. Sciortino, and P. Schurtenberger, *J. Phys. Chem. B* **115**, 7227 (2011).
- <sup>8</sup>S. Yadav, T. M. Laue, D. S. Kalonia, S. N. Singh, and S. J. Shire, *Mol. Pharm.* **9**, 791 (2012).
- <sup>9</sup>K. P. Johnston, J. A. Maynard, T. M. Truskett, A. U. Borwankar, M. A. Miller, B. K. Wilson, A. K. Dinin, T. A. Khan, and K. J. Kaczorowski, *ACS Nano* **6**, 1357 (2012).
- <sup>10</sup>J. C. F. Toledano, F. Sciortino, and E. Zaccarelli, *Soft Matter* **5**, 2390 (2009).
- <sup>11</sup>F. Sciortino, S. Mossa, E. Zaccarelli, and P. Tartaglia, *Phys. Rev. Lett.* **93**, 055701 (2004).
- <sup>12</sup>F. Sciortino, P. Tartaglia, and E. Zaccarelli, *J. Phys. Chem. B* **109**, 21942 (2005).
- <sup>13</sup>S. Mossa, F. Sciortino, P. Tartaglia, and E. Zaccarelli, *Langmuir* **20**, 10756 (2004).
- <sup>14</sup>P. Meakin, *Phys. Rev. Lett.* **51**, 1119 (1983).
- <sup>15</sup>M. Y. Lin, H. M. Lindsay, D. A. Weitz, R. C. Ball, R. Klein, and P. Meakin, *Nature (London)* **339**, 360 (1989).
- <sup>16</sup>C. L. Klix, C. P. Royall, and H. Tanaka, *Phys. Rev. Lett.* **104**, 165702 (2010).
- <sup>17</sup>H. Sedgwick, S. U. Egelhaaf, and W. C. K. Poon, *J. Phys.: Condens. Matter* **16**, S4913 (2004).

- <sup>18</sup>A. Campbell, V. Anderson, J. S. van Duijneveldt, and P. Bartlett, *Phys. Rev. Lett.* **94**, 208301 (2005).
- <sup>19</sup>P. Segrè, V. Prasad, A. Schofield, and D. A. Weitz, *Phys. Rev. Lett.* **86**, 6042 (2001).
- <sup>20</sup>E. J. Yearley, I. E. Zarraga, S. J. Shire, T. M. Scherer, Y. Gokarn, N. J. Wagner, and Y. Liu, *Biophys. J.* **105**, 720 (2013).
- <sup>21</sup>F. Cardinaux, A. Stradner, P. Schurtenberger, F. Sciortino, and E. Zaccarelli, *Europhys. Lett.* **77**, 48004 (2007).
- <sup>22</sup>S.-H. Chen, M. Broccio, Y. Liu, E. Fratini, and P. Baglioni, *J. Appl. Crystallogr.* **40**, s321 (2007).
- <sup>23</sup>Y. Liu, L. Porcar, J. Chen, W. Chen, P. Falus, A. Faraone, E. Fratini, K. Hong, and P. Baglioni, *J. Phys. Chem. B* **115**, 7238 (2011).
- <sup>24</sup>Y. Liu, W.-R. Chen, and S.-H. Chen, *J. Chem. Phys.* **122**, 044507 (2005).
- <sup>25</sup>M. Broccio, D. Costa, Y. Liu, and S.-H. Chen, *J. Chem. Phys.* **124**, 084501 (2006).
- <sup>26</sup>D. Costa, C. Caccamo, J.-M. Bomont, and J.-L. Bretonnet, *Mol. Phys.* **109**, 2845 (2011).
- <sup>27</sup>J.-M. Bomont, J.-L. Bretonnet, D. Costa, and J.-P. Hansen, *J. Chem. Phys.* **137**, 011101 (2012).
- <sup>28</sup>D. Frenkel and B. Smit, *Understanding Molecular Simulation* (Academic Press, 2002).
- <sup>29</sup>M. P. Allen and D. J. Tildesley, *Computer Simulation of Liquids* (Oxford University Press, 1987).
- <sup>30</sup>J.-M. Bomont, J.-L. Bretonnet, and D. Costa, *J. Chem. Phys.* **132**, 184508 (2010).
- <sup>31</sup>A. Shukla, E. Mylonas, E. Di Cola, S. Finet, P. Timmins, T. Narayanan, and D. I. Svergun, *Proc. Natl. Acad. Sci. U.S.A.* **105**, 5075 (2008).
- <sup>32</sup>M. E. Helgeson and N. J. Wagner, *J. Chem. Phys.* **135**, 084901 (2011).
- <sup>33</sup>M. G. Noro and D. Frenkel, *J. Chem. Phys.* **113**, 2941 (2000).
- <sup>34</sup>J. M. Kim, R. Castañeda-Priego, Y. Liu, and N. J. Wagner, *J. Chem. Phys.* **134**, 064904 (2011).
- <sup>35</sup>D. M. Heyes, M. Cass, and A. C. Brañka, *Mol. Phys.* **104**, 3137 (2006).
- <sup>36</sup>L. V. Woodcock, *AIChE J.* **58**, 1610 (2012).
- <sup>37</sup>D. Stauffer, *Phys. Rep.* **54**, 1 (1979).
- <sup>38</sup>S.-H. Chen, J. Rouch, F. Sciortino, and P. Tartaglia, *J. Phys.: Condens. Matter* **6**, 10855 (1994).
- <sup>39</sup>G. Nagele, *Phys. Rep.* **272**, 215 (1996).
- <sup>40</sup>N. A. Seaton and E. D. Glandt, *J. Chem. Phys.* **86**, 4668 (1987).
- <sup>41</sup>A. L. Benavides and A. Gil-villegas, *Mol. Phys.* **97**, 1225 (1999).
- <sup>42</sup>G. A. Chapela, F. del Río, A. L. Benavides, and J. Alejandre, *J. Chem. Phys.* **133**, 234107 (2010).
- <sup>43</sup>A. Vidales, A. L. Benavides, and A. Gil-villegas, *Mol. Phys.* **99**, 703 (2001).
- <sup>44</sup>J. Torres-Arenas, L. A. Cervantes, A. L. Benavides, G. A. Chapela, and F. del Río, *J. Chem. Phys.* **132**, 034501 (2010).
- <sup>45</sup>N. E. Valadez-Pérez, A. L. Benavides, E. Schöll-Paschinger, and R. Castañeda-Priego, *J. Chem. Phys.* **137**, 084905 (2012).
- <sup>46</sup>M. Miller and D. Frenkel, *J. Chem. Phys.* **121**, 535 (2004).
- <sup>47</sup>R. J. Baxter, *J. Chem. Phys.* **49**, 2770 (1968).
- <sup>48</sup>T. Jiang and J. Wu, *Phys. Rev. E* **80**, 021401 (2009).
- <sup>49</sup>A. Malins, S. R. Williams, J. Eggers, H. Tanaka, and C. P. Royall, *J. Non-Cryst. Solids* **357**, 760 (2011).
- <sup>50</sup>A. Coniglio, U. D. Angelis, and A. Forlani, *J. Phys. A* **10**, 1123 (1977).
- <sup>51</sup>Y. C. Chiew and E. D. Glandt, *J. Phys. A* **16**, 2599 (1983).
- <sup>52</sup>J. D. Martin, S. J. Goettler, N. Fossé, and L. Iton, *Nature (London)* **419**, 381 (2002).
- <sup>53</sup>C. S. Cundy and P. A. Cox, *Microporous Mesoporous Mater.* **82**, 1 (2005).
- <sup>54</sup>J. L. Provis and D. G. Vlachos, *J. Phys. Chem. B* **110**, 3098 (2006).
- <sup>55</sup>K. Kremer, M. O. Robbins, and G. S. Grest, *Phys. Rev. Lett.* **57**, 2694 (1986).
- <sup>56</sup>J.-P. Hansen and L. Verlet, *Phys. Rev.* **184**, 151 (1969).
- <sup>57</sup>L. L. Lee, M. C. Hara, S. J. Simon, F. S. Ramos, A. J. Winkle, and J.-M. Bomont, *J. Chem. Phys.* **132**, 074505 (2010).
- <sup>58</sup>P. D. Godfrin, R. Castañeda-Priego, Y. Liu, and N. J. Wagner, "Generalized phase behavior of cluster formation in colloidal dispersion with competing interactions," *Soft Matter* (unpublished).
- <sup>59</sup>P. Falus, L. Porcar, E. Fratini, W.-R. Chen, A. Faraone, K. Hong, P. Baglioni, and Y. Liu, *J. Phys.: Condens. Matter* **24**, 064114 (2012).
- <sup>60</sup>See supplementary material at <http://dx.doi.org/10.1063/1.4824487> for the cut-off distance dependence of hard sphere and HSDY system cluster size distribution and structure factor contributions as well as four movies demonstrating the real space structural dependence of connectivity on cut-off distance.